Yong Wan*, Wei-qing Chen and Shao-jie Wu

Effects of Lanthanum and Boron on the Microstructure and Magnetic Properties of Non-oriented Electrical Steels

Abstract: The effects of lanthanum and boron on the inclusion size distribution, microstructure, texture and magnetic properties of three non-oriented electrical steels have been studied. After final annealing, lanthanum effectively inhibited the precipitation of MnS precipitates and promoted the growth of grains, an addition of 0.0041 wt.% boron led to the precipitation of Fe_2B particles and inhibited grain growth. On the other hand, steel containing 0.0055 wt.% lanthanum had the strongest {100} and {111} fiber texture and the weakest {112}<110> texture among the steels. Compared to steel without lanthanum and boron, steel with 0.0050 wt.% lanthanum and 0.0041 wt.% boron obtained slightly stronger intensities of {100} and {111} fiber texture, and a little weaker intensity of {112}<110> texture. Steel containing 0.0055 wt.% lanthanum achieved the best magnetic properties, whose core loss and magnetic flux density were 4.268 W/kg and 1.768 T, respectively.

Keywords: lanthanum, boron, non-oriented electrical steel, grain size, texture, magnetic property

***Corresponding author: Yong Wan:** State Key Laboratory of Advanced Metallurgy, School of Metallurgical and Ecological Engineering, University of Science and Technology Beijing, Beijing 100083, China. E-mail: wanyong0729@163.com
Wei-qing Chen: State Key Laboratory of Advanced Metallurgy, School of Metallurgical and Ecological Engineering, University of Science and Technology Beijing, Beijing 100083, China
Shao-jie Wu: State Key Laboratory of Advanced Metallurgy, School of Metallurgical and Ecological Engineering, University of Science and Technology Beijing, Beijing 100083, China; Technology Center of Xinyu Iron and Steel Co., Ltd., Xinyu 338001, China

1 Introduction

Non-oriented electrical steels are widely used for core materials of rotating machines. In order to make rotating machines smaller and of higher efficiency, magnetic properties of core materials should be improved. In many applications of non-oriented electrical steels, low core loss and high permeability are the most important requirements. Therefore, much research is devoted to the study and development of low core loss and high magnetic induction electrical steels. Some key factors, such as chemical composition, impurities, inclusions, grain size, and texture determine the magnetic properties of non-oriented electrical steels [1–4]. It is well known that manganese sulfide and aluminum nitride inclusions in the size range of 10–400 nm are deleterious to magnetic properties, either directly by impeding the magnetic domain movement, or indirectly through refining the grain size during final annealing [5, 6]. Rare earth elements have strong mutual chemical affinity with sulfur and oxygen and tend to form high melting point oxides, oxysulfides and sulfides [7–9]. Hou [10] found that increasing the cerium content from 0 wt.% to 0.022 wt.% could reduce inclusion density in the whole size range for non-oriented electrical steel. Lyudkovksy [11] found that adding 0.0007–0.0038 wt.% boron into Al-killed low carbon steels containing 0.033–0.053 wt.% aluminum could inhibit precipitation of A1N precipitates through enhanced precipitation of BN precipitates, in both cases, improved crystallographic texture and grain size contributed to enhanced magnetic permeability of the final product. So far, there are no reports that thoroughly studied the compound addition of rare earth and boron elements on the magnetic properties of high aluminum non-oriented electrical steels. This fact stimulated us to systematically study the effects of lanthanum and boron on the inclusion type, microstructure, texture and magnetic properties of high aluminum non-oriented electrical steels.

2 Experimental procedures

Three non-oriented electrical steels with varing chemical compositions were melted in a vacuum induction furnace at a temperature of 1600 °C and were cast into 6.5 kg ingots. The chemical compositions are shown in Table 1. The ingots were first reheated at 1150 °C for 2 h in a heating furnace, then an air forging hammer was used to forge

Table 1: Chemical compositions of all the tested steels (wt.%)

Steels	C	Si	Mn	S	P	Als	T[O]	N	La	Bs
1	0.0038	1.36	0.36	0.0037	0.027	0.36	0.0024	0.0048	0	0
2	0.0053	1.49	0.35	0.0039	0.027	0.37	0.0023	0.0047	0.0055	0
3	0.0060	1.29	0.36	0.0043	0.027	0.35	0.0024	0.0055	0.0050	0.0041

them into 70 mm × 80 mm × 100 mm ingots. The forged ingots were reheated to 1150 °C for 2 h and hot-rolled in two steps by a two-high pilot hot rolling mill. The thickness of steel ingots after rough rolling was 22 mm and after finishing rolling was 2.5 mm. Two levels of hot-rolled finishing temperature were conducted at 850–890 °C. After air cooling to room temperature, hot-rolled bands were normalized at 950 °C for 5 min and cooled in the air. Then, the normalized hot-rolled bands were pickled and cold rolled to a thickness of 0.50 mm with a total reduction of 80% by a four-high-pilot cold rolling mill. Then, the cold-rolled steel sheets were cut into 300 mm × 30 mm specimens both in longitudinal and transverse direction with respect to the rolling direction. Finally, the specimens were annealed in a continuous annealing furnace set at 920 °C for 3 min in an atmosphere of 30% H_2 and 70% N_2, and finally cooled in the furnace.

After cold-rolling and final annealing, each specimen was analyzed to measure {110}, {200} and {211} pole figures using a Siemens D-5000 X-ray diffractometer with a texture attachment. The diffractometer used Mo radiation and was operated at 40 kV and 25 mA. Then three pole figure data was used to calculate the orientation distribution by ODF software with L = 22. Magnetic properties of the specimens were measured using a Soken DACBHW-2 electrical steel tester. Magnetic flux density was measured at 5000 A/m field strength and ac core loss was measured at 15 kg induction and 50 Hz, respectively. Both longitudinal and transverse specimens were measured and their values were averaged. Microstructures of finally annealed cold-rolled steel sheets were observed by optical microscope and image analyzer. Grain size of the cold-rolled steel sheets after final annealing was measured by using the intercept method based on ASTM standard E-112. To measure the number and size distribution of inclusions with size more than 1 μm in the annealed cold-rolled bands, specimens were examined using a JSM-6480LV scanning electron microscope (SEM) at 1000× magnification. The number and size distribution of inclusions with size less than 1 μm were observed using a ZEISS ULTRA 55 field scanning electron microscope (FSEM) at 14000× magnification. Fifty field images of each specimen were taken and the size and number of inclusions were measured using a Leco IA3-001 image analysis system. Inclusion density is here defined as the total inclusion number divided by the total counted area.

3 Results and discussion

3.1 Thermodynamic considerations of inclusion forming reactions

The deoxidation and desulfuration reactions [12] of lanthanum and the standard Gibbs free energies of formation of some La compounds in liquid iron are shown in Fig. 1(a). The interaction coefficients of other elements on O, S and La in liquid steel at 1600 °C are summarized in Table 2 [12–15]. The values of Raoultian activities of La_2O_3, La_2O_2S, La_2S_3 and LaS are assumed to be 1 in the present study. Based on Table 2, the chemical compositions of steel 2 and Fig. 1(a), the Gibbs free energies of formation of some La compounds at 1600 °C are calculated as shown in Fig. 1(b). It can be seen that the Gibbs free energies of formation of La_2O_2S and LaS are smaller than that of La_2O_3 and La_2S_3 at 1600 °C in steel 2, respectively, which means that La_2O_3 and La_2S_3 are unstable and liable to transform into La_2O_2S and LaS at 1600 °C, respectively.

The relationships between the content of BN, AlN type precipitates and temperature in steel 3, which are calculated by the solid solubility formulas of BN and AlN in thermal equilibrium state [16, 17], are shown in Fig. 2. It can be seen that the starting precipitation temperature of AlN type precipitates is significantly higher than that of BN type precipitates, which indicates that aluminum can combine with free nitrogen preferentially to form coarse AlN particles. As the concentration of acid-soluble aluminum (= 0.35 wt.%) is very high, aluminum is enough to react with nitrogen, there is no free nitrogen left in the sample, and as a result, the precipitation of BN is restrained sufficiently. Therefore, boron is believed to segregate on the grain boundaries or form additional boron containing compounds in steel.

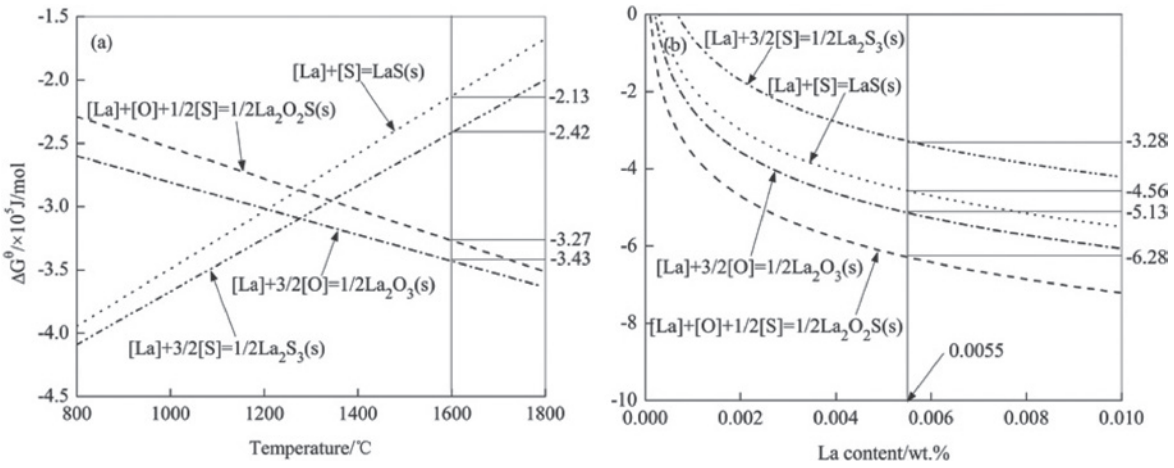

Fig. 1: The Gibbs free energies of formation of some La compounds in liquid iron: (a) the standard Gibbs free energies as a function of temperature; (b) the Gibbs free energies as a function of La content at 1600 °C

Table 2: Interaction coefficient of each element in liquid steel at 1600 °C

$e_i^j(j)$	C	Si	Mn	P	S	Al	O	La
O	−0.42	−0.066	−0.0224	0.07	−0.133	−1.17	−0.17	−5
S	0.112	0.063	−0.026	0.29	−0.028	0.035	−0.27	−4.8
La	−0.33	–	–	–	−12.13	–	−43.47	−0.0078

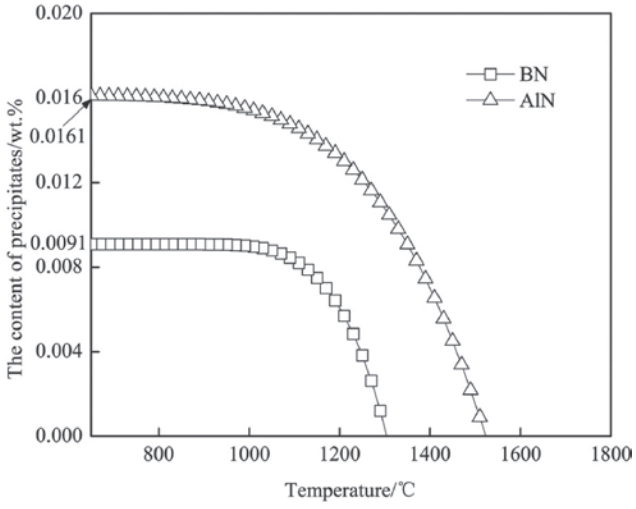

Fig. 2: The relationships between the content of BN, AlN precipitates and temperature

3.2 Inclusion size distribution

The inclusion size distribution of annealed cold-rolled steel sheets for the tested steels is shown in Fig. 3. From Fig. 3(a), the micro-inclusions are mainly in the size range of 1–5 μm. Steel 1 has the lowest inclusion density with size more than 1 μm. Steel 3 has the highest inclusion density in the size range of 1–3 μm. Furthermore, the average diameter of micro-inclusions with size more than 1 μm in steel 3 is smaller than that in the other two steels. Fig. 3(b) shows the fine inclusion size distribution in the range of 0–1 μm for the three tested steels. It is found that the fine inclusions are mainly in the size range of 0.03–0.15 μm. Steel 1 has the highest inclusion density with size less than 1 μm. Its distribution has a peak inclusion density value in the size range of 0.05–0.08 μm. Steel 2 has lower inclusion density in the size range of 0.05–0.08 μm than steel 3. Furthermore, steel 2 has the greatest average diameter of fine inclusions compared to the other steels. It can be observed that numerous LaS and La_2O_2S inclusions in the size range of 1–3 μm exist in steel 2 and 3, and a handful of Fe_2B particles exist in steel 3 as shown in Fig. 4. As stated above, it is postulated that lanthanum effectively inhibits the precipitation of MnS precipitates, an excessive addition of boron(>0.0041 wt.%) may result in the formation of additional boron containing compounds(e.g. Fe_2B) in steel.

3.3 Grain size of annealed cold-rolled steel sheets

The optical microstructures and average grain sizes of annealed cold-rolled steel sheets for the tested steels are shown in Figs. 5 and 6. At the same processing conditions,

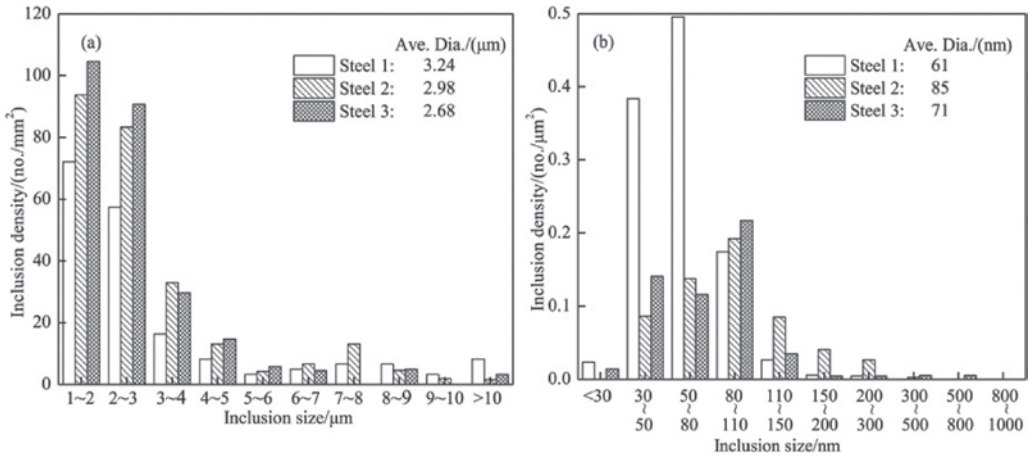

Fig. 3: Inclusion size distribution in tested steels: (a) inclusion distribution for size more than 1 μm; (b) inclusion distribution for size less than 1 μm

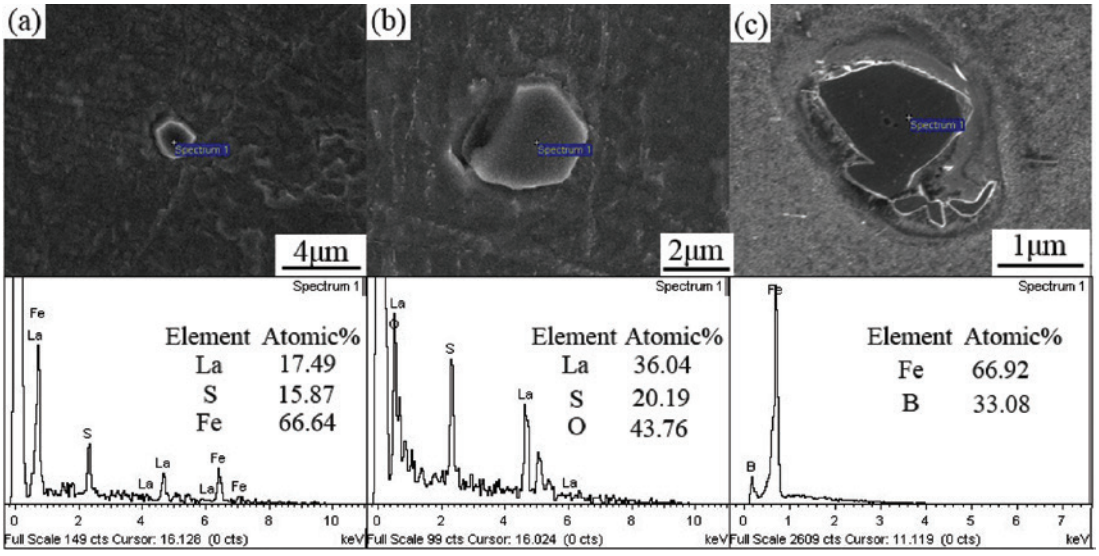

Fig. 4: FSEM images and EDS spectra of inclusions in the tested steels: (a) LaS; (b) La_2O_2S; (c) Fe_2B

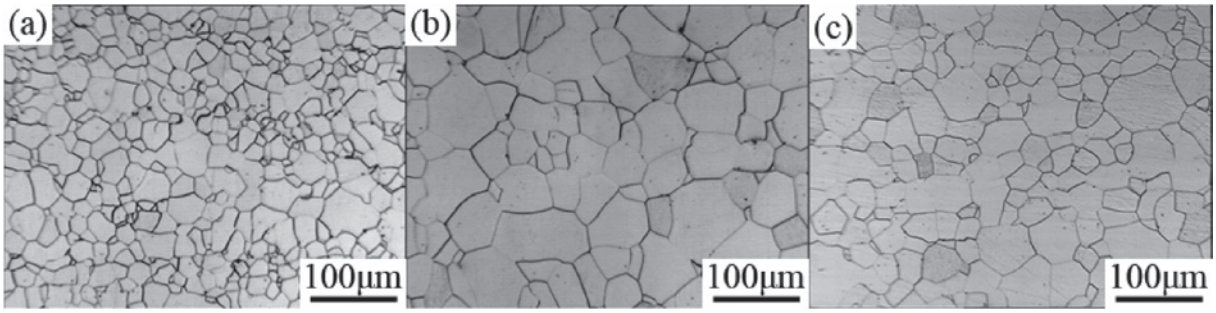

Fig. 5: Optical microstructures of annealed cold-rolled steel sheets: (a) steel 1; (b) steel 2; (c) steel 3

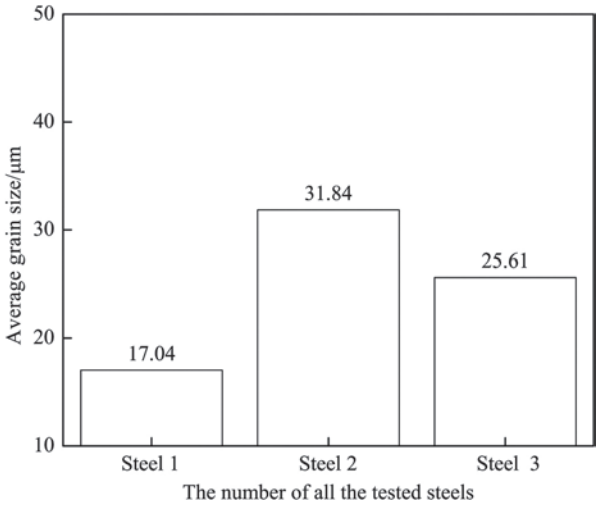

Fig. 6: Average grain size of annealed cold-rolled steel sheets: (a) steel 1; (b) steel 2; (c) steel 3

steel 2 obtains the largest grain size among the tested steels. Steel 1 has the smallest grain size. Many factors, such as inclusion volume fraction, inclusion size, cold rolled reduction, and continuous annealing temperature and time affect the final grain size of non-oriented electrical steels. In this study, the cold rolled reduction, and continuous annealing temperature and time are kept constant. Therefore, the population density and size of inclusion play very important roles. According to Zener theory, the inhibition strength against grain growth is proportional to the volume fraction of inclusions and is inversely proportional to average inclusion radius. Therefore, fine inclusions more effectively impede grain growth in non-oriented electrical steels during recrystallization. As mentioned previously, steel 1 has the most fine MnS inclusions with size less than 0.08 μm. Therefore, it has the smallest grain size after final annealing. Compared to steel 3, steel 2 has greater average inclusion size and inexistence of Fe_2B precipitates. This is the reason that steel 2 obtains the largest grain size after final annealing.

3.4 Texture

The main low index orientations of cubic structure materials in the Euler space are located at the orientation distribution function maps at $\varphi_2 = 0°$ and $\varphi_2 = 45°$ as shown in Fig. 7. The effects of lanthanum and boron on the orientation distribution function of final annealed steel sheets are shown in Fig. 8. The main preferred orientations of all the annealed specimens are {111}<110>, {111}<112>, {110}<001>, {001}<100> and {112}<110>. Fig. 9 shows the effects of lanthanum and boron on the annealing texture with intensities along the alpha and gamma fiber. The volume fractions of three fiber texture components of annealed cold-rolled steel sheets are shown in Table 3. It can be seen that steel 2 obtains the strongest intensities of {100} and {111} fiber texture, and the weakest intensity of {112}<110> texture among the tested steels. Compared to steel 1, steel 3 has slightly stronger intensities of {100} and {111} fiber texture, and a little weaker intensity of {112}<110> texture. The analysis of texture data mentioned above indicates that the presence of a handful of lanthanum in non-oriented electrical steel are conducive to the development of the {100} and {111} fiber texture component at the expense of the {112}<110> texture component. However, an addition of boron content exceeding 0.0041 wt.% is believed to produce the opposite effect.

3.5 Magnetic properties

The effects of lanthanum and boron on the core loss and magnetic flux density in non-oriented electrical steels after final annealing are shown in Table 4. Among the

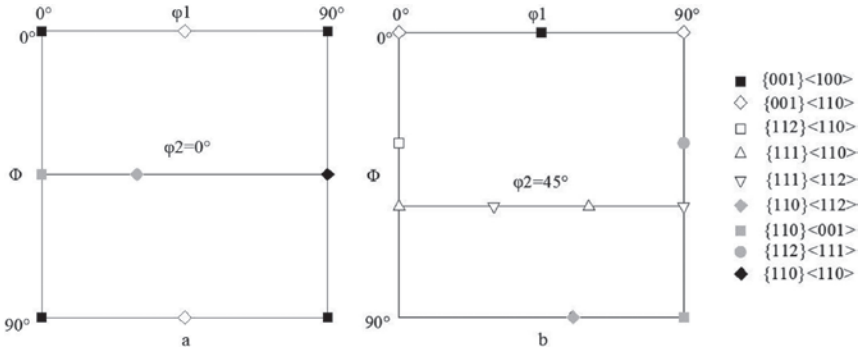

Fig. 7: Ideal preferred orientation in the Euler space: (a) $\varphi_2 = 0°$; (b) $\varphi_2 = 45°$

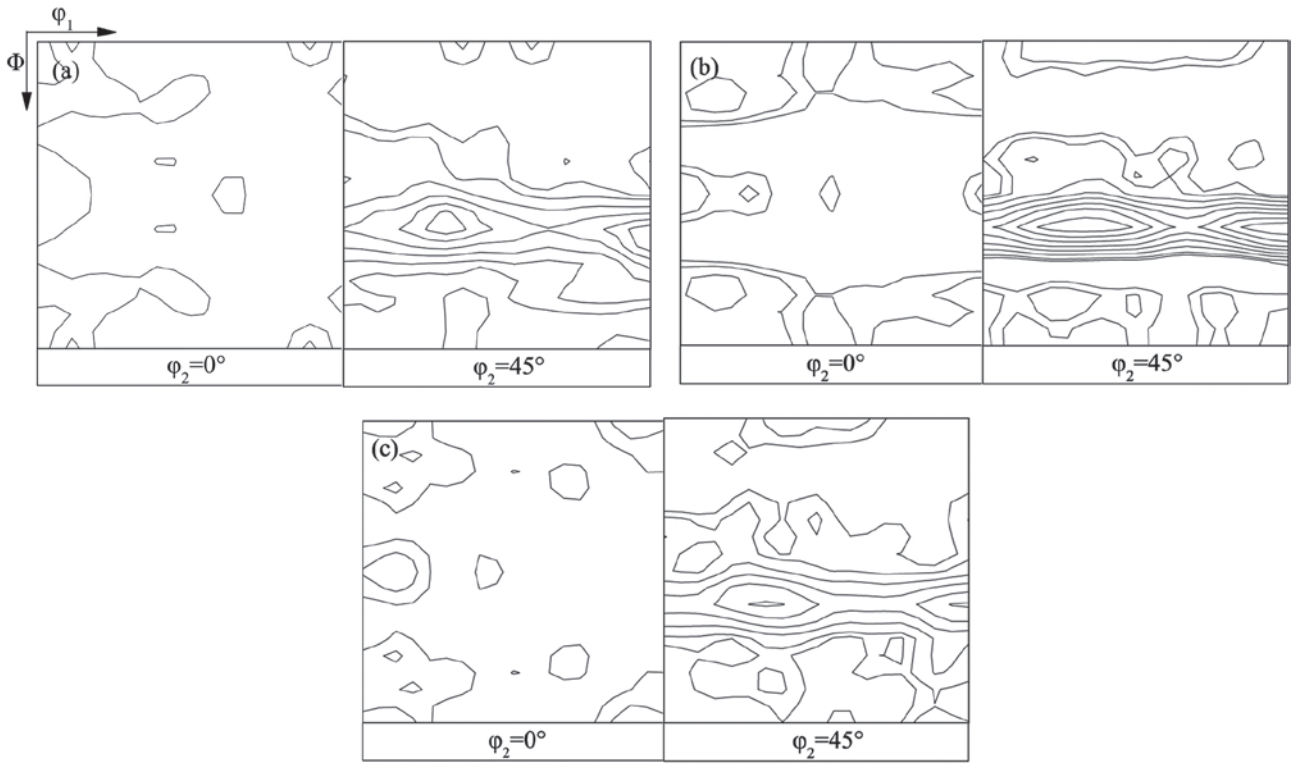

Fig. 8: ODF section views of annealed cold-rolled steel sheets: (a) steel 1; (b) steel 2; (c) steel 3 (levels: 1, 2, 4, 6, 8, 10, 12, 14, 16)

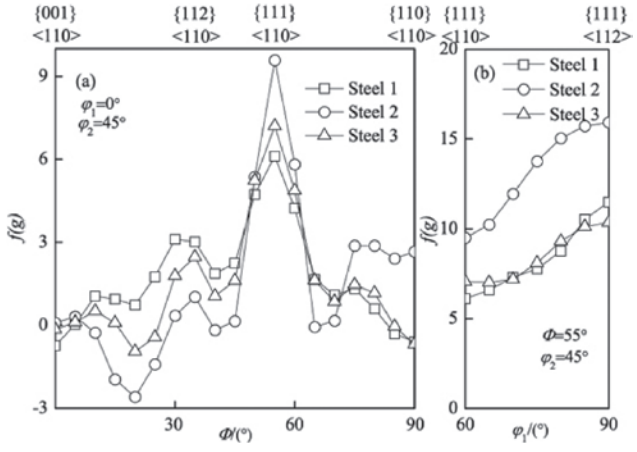

Fig. 9: Orientation distribution intensities of annealed cold-rolled steel sheets as a function of (a) Φ along α fiber and (b) φ_1 along γ fiber

Table 3: The volume fractions of three fiber texture components of annealed cold-rolled steel sheets (%)

Steels	{100} fiber texture	Goss texture	{111} fiber texture
1	1.63	3.31	14.39
2	5.46	3.44	17.38
3	2.32	3.40	14.10

Table 4: Core loss and magnetic flux density of annealed cold-rolled steel sheets

Steels	$P_{15/50}$ (W/kg)	B_{50} (T)
1	4.81	1.747
2	4.268	1.768
3	4.588	1.757

three tested steels, steel 1 has the highest core loss and the lowest magnetic flux density, steel 2 obtains the lowest core loss and the highest magnetic flux density. Grain boundaries represent a barrier that impedes domain movement during magnetization. Therefore, coarse grain size is a benefit in decreasing hysteresis loss and core loss. On the other hand, coarse grain size induces large domain sizes and large eddy current losses. Therefore, there is an optimum grain size to achieve minimum core loss. Another factor that influences the core loss is population and size of inclusions. Since inclusions impede domain movement during magnetization, they lead to increase in the hysteresis loss and core loss. It has been reported that the large (>0.5 μm) and the very fine (<0.05 μm) inclusions are less harmful to the magnetic properties than the 0.05–0.5 μm sized ones [18]. As stated above, steel 1 has the largest population density of fine inclusions in the size range of

0.05–0.08 μm and the smallest grain size. Therefore, it obtains a maximum in core loss. Compared to steel 3, steel 2 has larger grain size, lower quantity of micro-inclusions and fine inclusions, and achieves lower core loss. A significant factor that influences magnetic flux density is the crystallographic texture component. It is well known that the <100> crystallographic axis of α-iron is the easiest magnetization direction. However, the <111> crystallographic axis is the most difficult magnetization direction. Both (001) and (011) crystallographic planes contain the easy magnetization direction and are favorable to the magnetic properties of non-oriented electrical steels. However, the (111) and (112) crystallographic plane does not contain any easy magnetization axis. As mentioned previously, the steel 2 has the strongest {100} fiber texture and the weakest {112}<110> texture among the tested steels, therefore, it obtains the highest flux density.

4 Conclusions

1. After final annealing, an addition of 0.0055 wt.% lanthanum in steel effectively inhibited the precipitation of MnS precipitates and promoted the growth of grains, an addition of 0.0041 wt.% boron led to the precipitation of Fe_2B particles and inhibited grain growth.
2. Among the three tested steels, steel containing 0.0055 wt.% lanthanum obtains the largest grain size, whose grain size are 31.84 μm.
3. Compared to steel without lanthanum and boron, steel with 0.0050 wt.% lanthanum and 0.0041 wt.% boron obtains slightly stronger intensities of {100} and {111} fiber texture, and a little weaker intensity of {112}<110> texture. Steel containing 0.0055 wt.% lanthanum has the strongest {100} and {111} fiber texture and the weakest {112}<110> texture among the steels.
4. Among the three tested steels, steel without lanthanum and boron has the highest core loss and the lowest magnetic flux density, steel containing 0.0055 wt.% lanthanum obtains the lowest core loss and the highest magnetic flux density.

Acknowledgments: The authors are grateful for financial support by the Xinyu Iron and Steel Company of China.

Received: April 22, 2013. Accepted: June 14, 2013.

References

[1] M. F. Littmann, Iron and silicon-iron alloys. *IEEE Trans. Mag.*, 7(1971), No. 1, p. 48.
[2] C. K. Hou, C. T. Hu, S. Lee, The effect of aluminum on the magnetic properties of lamination steels, *IEEE Trans. Mag.*, 27(1991), No. 5, p. 4305.
[3] C. K. Hou, The effects of grain size on the magnetic properties of fully processed, continuous-annealed low-carbon electrical steels, *IEEE Trans. Mag.*, 32(1996), No. 2, p. 471.
[4] E. T. Stephenson, A. R. Marder, The effects of grain size on the core loss and permeability of motor lamination steel, *IEEE Trans. Mag.*, 22(1986), No. 2, p. 101.
[5] P. Beckley, J. E. Thompson, Influence of inclusions on domain-wall motion and power loss in oriented electrical steel, *Proc. IEE.*, 117(1970), No. 11, p. 2194.
[6] M. Shiozaki, Y. Kurosaki, The effects of grain size on the magnetic properties of non-oriented electrical steel sheets, *J. Mater. Eng.*, 11(1989), No. 1, p. 37.
[7] L. Luyckx, J. R. Bell, A. Mclean, M. Korchynsky, Sulfide shape control in high strength low alloy steels, *Metall. Mater. Trans. B*, 1(1970), No. 12, p. 3341.
[8] W. G. Wilson, R. G. Wells, Identifying inclusions in rare earth treated steels, *Met. Prog.*, 104(1973), No. 12, p. 75.
[9] W. G. Wilson, D. A. Kay, A. Vahed, The use of thermodynamics and phase equilibria to predict the behavior of the rare earth elements in steel, *J. Met.*, 26(1974), No. 3, p. 14.
[10] C. K. Hou, C. C. Liao, Effect of cerium content on the magnetic properties of non-oriented electrical steels, *ISIJ Int*, 48(2008), No. 4, p. 531.
[11] G. Lyudkovksy, P. K. Rastogi, Effects of boron and zirconium on microstructure and magnetic properties of batch annealed Al-killed low carbon steels, *IEEE Trans. Mag.*, 21(1985), No. 5, p. 1912.
[12] D. Chen, Q. Y. Han, T. Wang, C. X. Xiang, Thermodynamics of Fe-La-S-O metallic solution. *Acta Metallurgica Sinica* (in Chin.), 22(1986), No. 2, p. 156.
[13] L. M. Wang, T. Du, Y. M. Wu, Thermodynamics of the formation of RE_S and RE_2S_3 in steel, *Rare Earth* (in Chin.), (1987), No. 6, p. 11.
[14] L. M. Wang, T. Du, X. L. Lu, Z. B. Li, Y. C. Gai, Thermodynamics and application of rare earth elements in steel, *Rare Earth* (in Chin.), 21(2003), No. 3, p. 251.
[15] A. Vahed, D. A. R. Kay, Thermodynamics of rare earths in steelmaking. *Metall. Mater. Trans. B*, 7(1976), No. 3, p. 375.
[16] H. C. Fiedler, The solubility product of boron nitride in 3.1 pct silicon-iron, *Metall. Mater. Trans. A*, 9(1978), No. 10, p. 1489.
[17] L. A. Erasmus, Effect of aluminum additions on forgeability, austenite grain coarsening temperature, and impact properties of steel, *ISIJ Int*, 202(1964), No. 1, p. 32.
[18] I. Boc, A. Cziraki, T. Grof, J. Csebi, Analysis of inclusions in cold-rolled n.o. Si-Fe Strips, *J. Magn. Magn. Mater*, 83(1990), No. 1–3, p. 381.